An active dimanganese(III)-tyrosyl radical cofactor in Escherichia coli class Ib ribonucleotide reductase

Published in final edited form as:
Biochemistry. 2010 February 16; 49(6): 1297–1309. doi:10.1021/bi902106n.

An active dimanganese(III)-tyrosyl radical cofactor in *Escherichia coli* class Ib ribonucleotide reductase†

Joseph A. Cotruvo Jr[‡] and **JoAnne Stubbe**[‡,§,*]

[‡]Department of Chemistry, Massachusetts Institute of Technology, Cambridge, MA 02139

[§]Department of Biology, Massachusetts Institute of Technology, Cambridge, MA 02139

Abstract

Escherichia coli class Ib ribonucleotide reductase (RNR) converts nucleoside 5′-diphosphates to deoxynucleoside 5′-diphosphates and is expressed in iron-limited and oxidative stress conditions. This RNR is composed of two homodimeric subunits: α2 (NrdE), where nucleotide reduction occurs, and β2 (NrdF), which contains an unidentified metallocofactor that initiates nucleotide reduction. *nrdE* and *nrdF* are found in an operon with *nrdI*, which encodes an unusual flavodoxin proposed to be involved in metallocofactor biosynthesis and/or maintenance. Ni affinity chromatography of a mixture of *E. coli* $(His)_6$-NrdI and NrdF demonstrated tight association between these proteins. To explore the function of NrdI and identify the metallocofactor, apoNrdF was loaded with Mn^{II} and incubated with fully reduced NrdI ($NrdI_{hq}$) and O_2. Active RNR was rapidly produced with 0.25 ± 0.03 tyrosyl radical (Y•) per β2 and a specific activity of 600 U/mg. EPR and biochemical studies of the reconstituted cofactor suggest it is Mn^{III}_2-Y•, which we propose is generated by Mn^{II}_2-NrdF reacting with two equivalents of HO_2^-, produced by reduction of O_2 by NrdF-bound $NrdI_{hq}$. In the absence of $NrdI_{hq}$, with a variety of oxidants, no active RNR was generated. By contrast, a similar experiment with apoNrdF loaded with Fe^{II} and incubated with O_2 in the presence or absence of $NrdI_{hq}$ gave 0.2 and 0.7 Y•/β2 with specific activities of 80 and 300 U/mg, respectively. Thus $NrdI_{hq}$ hinders Fe^{III}_2-Y• cofactor assembly in vitro. We propose that NrdI is an essential player in *E. coli* class Ib RNR cluster assembly and that the Mn^{III}_2-Y• cofactor, not the diferric-Y• one, is the active metallocofactor in vivo.

Ribonucleotide reductases (RNRs) catalyze the conversion of nucleotides to deoxynucleotides in all organisms, supplying and controlling the pool of deoxynucleotides (dNTPs[1]) required for DNA replication and repair (1). Class I RNRs are composed of two homodimeric subunits: α2, which contains the site of nucleotide reduction, and β2, which harbors the metallocofactor required for initiation of nucleotide reduction. *Escherichia coli* (*Ec*) possesses two RNRs that are differentially expressed in aerobic growth. Its class Ia RNR, NrdA (α2) and NrdB (β2), supplies and controls pools of dNTPs needed for DNA biosynthesis under normal growth conditions. The function of the class Ib RNR, NrdE [α2 (2)] and NrdF (β2), is not well understood, but the enzyme is expressed under iron-limited

†This research was supported by National Institutes of Health grant GM81393 to J.S. and a National Defense Science and Engineering Graduate (NDSEG) fellowship to J.A.C.

*To whom correspondence should be addressed., Tel: (617) 253-1814., Fax: (617) 324-0505., stubbe@mit.edu.

SUPPORTING INFORMATION AVAILABLE

Additional experimental details and results: Cluster assembly in the presence of SOD or catalase, efforts to determine the oxidant generated by reaction of $NrdI_{hq}$ and O_2, reconstitutions of Mn^{II}_2-NrdF with H_2O_2 and $O_2^{\bullet-}$ as oxidants, further EPR studies to determine the oxidation state of the dimanganese cluster in active NrdF, investigation of whether $NrdI_{hq}$ reduces Mn^{III}_2-Y• and Mn^{III}_2-NrdF, visible spectra of titrations of NrdI in the presence and absence of NrdF, EPR spectra of the anionic and neutral sq forms of NrdI, and EPR spectrum (1800–4800 G) of Mn^{III}_2-Y• NrdF at 3.6 K. This material is available free of charge via the Internet at http://pubs.acs.org.

and oxidative stress conditions (3–6). However, for many prokaryotes – including the human pathogens *Mycobacterium tuberculosis* (*Mt*), *Bacillus anthracis* (*Ba*), and *Staphylococcus aureus* – class Ib RNRs supply the dNTPs used in DNA biosynthesis in aerobic growth conditions (7). While the class Ia RNRs require a diferric-tyrosyl radical (Fe^{III}_2-Y•) cofactor for activity, the nature of the class Ib RNR's metallocofactor is controversial (8–16). The present work describes our efforts to identify the active form of the metallocofactor of the *E. coli* class Ib RNR.

Initial in vivo and in vitro studies of the class Ib RNR metallocofactor were carried out in *Corynebacterium ammoniagenes* (*Ca*), which possesses only a class Ib enzyme. Early experiments demonstrated that *C. ammoniagenes* required manganese for growth (17), and biochemical studies of the *Ca* RNR purified from endogenous levels (8, 9) led Follmann and Auling to propose a Mn^{III}_2-Y• cofactor (10). The isolated NrdF protein, however, had a specific activity (SA) of 0.7 nmol dCDP produced/min/mg (U/mg) protein, <0.01% that of the purified *Ec* class Ia β2 (NrdB), and no detectable Y• (10). The amounts of NrdF isolated were insufficient for biophysical characterization of the active cofactor (10, 13). Very recently, Auling, Pierik, and coworkers have reported that the NrdF purified from *Corynebacterium glutamicum* contains Mn, possesses a SA of 32000 U/mg (>400% of *Ec* NrdB), and has an EPR spectrum consistent with the presence of an organic radical (14). However, the structure of the active cofactor was not specified. *E. coli* also requires Mn for growth when all known Fe uptake systems are deleted and the resulting strain (GR536) is grown in minimal media in the presence of Fe chelators (18). Although the origin of this Mn requirement is unknown, the class Ib RNR is expressed in these conditions (Cotruvo and Stubbe, unpublished results). Finally, studies by Imlay and coworkers have recently established that *E. coli* requires Mn under conditions of chronic H_2O_2 stress (19), another condition in which *nrdEF* transcript levels are increased (5).

By contrast, other studies have demonstrated activity of a Fe^{III}_2-Y• cofactor in NrdF. Sequence alignments of the class Ib and Ia RNRs and a comparison of their crystal structures reveal that they possess the same metal ligands and a tyrosine residue (Y_{105} in *Ec* NrdF) in the appropriate position for oxidation (20, 21). Metallocofactor self-assembly studies in apoNrdFs from several organisms have been carried out, modeled after those of Atkin and Reichard (22) on the class Ia NrdB. In these experiments, apoNrdF, Fe^{II}, and O_2 were able to form a Fe^{III}_2-Y• cofactor that was active in nucleotide reduction. Some NrdFs also co-purify with a Fe^{III}_2-Y• cofactor when overexpressed heterologously in *E. coli* in rich media. For example, heterologous expression of *Salmonella typhimurium* (*St*) NrdF in *E. coli* resulted in NrdF with 1 Y•/β2 and a SA of 660–850 U/mg (11, 12), while cofactor self-assembly in vitro from apoNrdF gave 0.4 Y•/β2 and 325 U/mg SA (11). In general, however, Fe^{III}_2-Y• NrdFs assembled in vitro or in vivo possess ≤0.5 Y•/β2 and/or activities of <200 U/mg [Table S1 in (23)]. Conversely, efforts to self-assemble an active manganese cofactor in *St* and *Ca* NrdFs using Mn^{II} and the physiological oxidants O_2 and H_2O_2 failed to generate significant Y• and activity (11). As a result of these experiments, the Fe^{III}_2-Y• has been proposed to be the active cofactor in the class Ib β2s (11, 12).

[1]Abbreviations: α2, ribonucleotide reductase large subunit; β2, ribonucleotide reductase small subunit; *Ba*, *Bacillus anthracis; Ca*, *Corynebacterium ammoniagenes*; CDP, cytidine 5′-diphosphate; CV, column volumes; dATP, deoxyadenosine 5′-triphosphate; DEPMPO, 5-(diethoxyphosphoryl)-5-methyl-1-pyrroline *N*-oxide; dNTP, deoxynucleoside 5′-triphosphate; *Ec*, *Escherichia coli;* EDTA, ethylenediaminetetraacetic acid; GR536, *E. coli* strain with deletions in the five known iron uptake pathways; HU, hydroxyurea; met-NrdF, tyrosyl radical-reduced diferric NrdF; *Mt*, *Mycobacterium tuberculosis*; N•, nitrogen-centered radical; N_3CDP, 2′-azido-2′-deoxycytidine 5′-diphosphate; Ni-NTA, nickel nitrilotriacetic acid; $NrdI_{hq}$, NrdI hydroquinone form; $NrdI_{ox}$, oxidized NrdI; $NrdI_{sq}$, NrdI semiquinone form; RNR, ribonucleotide reductase; SA, specific activity; SDS-PAGE, sodium dodecyl sulfate–polyacrylamide gel electrophoresis; SOD, superoxide dismutase; *St*, *Salmonella typhimurium*; $W^{+\bullet}$, tryptophan cation radical; Y•, tyrosyl radical

Our efforts have recently focused on understanding the biosynthesis and maintenance (regeneration of Y• from inactive, Y•-reduced protein) of the metallocofactors of the *E. coli* class Ia and Ib RNRs. Analyses of operons of these RNRs (http://theseed.uchicago.edu) and in vitro experiments have revealed that an unusual ferredoxin, YfaE, in the case of class Ia (24, 25), and an unusual flavodoxin, NrdI, in the case of class Ib (23), are involved in some way in these pathways in *E. coli*. Indeed, class Ia and Ib RNRs are distinguished, in part, by the presence of *nrdI*, often in the same operon as *nrdE* and *nrdF*. Recent genetic studies of the class Ib RNR from *Streptococcus pyogenes*, which does not possess a class Ia enzyme, demonstrated that NrdI is essential for NrdEF activity in vivo (26).

These studies together have caused us to reinvestigate, in vitro and in vivo, whether a dimanganese-Y• cofactor could be active in nucleotide reduction in the class Ib RNR, with NrdI supplying the oxidant required for metallocofactor assembly. Here we show that NrdI interacts strongly with NrdF and we report the first in vitro generation of a dimanganese-Y• cofactor in *Ec* NrdF. This reconstitution was successful only when dimanganese(II) NrdF (Mn^{II}_2-NrdF) was incubated anaerobically with the two-electron reduced, hydroquinone form of NrdI ($NrdI_{hq}$), followed by addition of O_2. A dimanganese-Y• cofactor (0.25 Y•/β2) was generated with a SA of 600 U/mg. EPR analysis supports the proposal that this cofactor is Mn^{III}_2-Y• and that the Y• interacts with the metal center. While $NrdI_{hq}$ is essential for Mn^{III}_2-Y• cofactor generation in vitro, it interferes with Fe^{III}_2-Y• cofactor formation. Self-assembly experiments carried out with Fe^{II}_2-NrdF and O_2, in the presence and absence of $NrdI_{hq}$, generated a Fe^{III}_2-Y• cofactor with 0.2 and 0.7 Y•/β2 and SAs of 80 and 300 U/mg, respectively.

Our experiments support the hypothesis that $NrdI_{hq}$ provides the oxidant required for assembly of the Mn^{III}_2-Y• cofactor in NrdF by reacting with O_2 to produce HO_2^-. Such a role is, to our knowledge, unprecedented for a flavodoxin-like protein, although not uncommon in other classes of flavoenzymes (27). We suggest that this function provides a general explanation for the role of NrdI in vivo, and that the Mn^{III}_2-Y• cofactor may also be the active form of class Ib RNRs inside the cell. More generally, our results emphasize that in vitro study of metalloproteins must consider their in vivo expression conditions so that the physiologically important metallocofactor is identified.

MATERIALS AND METHODS

General

Chemical reagents were obtained from Sigma-Aldrich in the highest purity available unless otherwise indicated. 2′-Azido-2′-deoxycytidine 5′-diphosphate (N_3CDP) was synthesized as described (28, 29). UV-vis spectra were acquired on a Varian Cary 3 UV-vis spectrophotometer. Anaerobic procedures were carried out in a glovebox (MBraun) in a cold room at 4 °C. Protein solutions and buffers for anaerobic work were degassed on a Schlenk line with 5–6 cycles (protein) or 3 cycles (buffer) of evacuation and refilling with Ar prior to introduction into the glovebox. Manganese concentrations were determined using a Perkin-Elmer AAnalyst 600 atomic absorption spectrometer, and iron was quantitated by the ferrozine method (30). Solutions of H_2O_2 [ε_{230nm} = 72.8 M^{-1} cm^{-1} (31)] were prepared immediately before use by dilution of a 30% H_2O_2 stock solution. Concentrations of NrdF and NrdI are given per dimer (β2) and monomer, respectively.

Buffers

The SA of the Mn^{III}_2-Y• cofactor was highest when assembled in 50 mM HEPES, 5% glycerol, pH 7.6 (**Buffer A**). However, NrdI was poorly soluble in Buffer A at concentrations >30 μM; therefore, most experiments were carried out in 50 mM sodium

phosphate, 5% glycerol, pH 7.6 (**Buffer B**). O_2-saturated Buffers A and B (~1.9 mM O_2) were prepared immediately prior to use at 4°C by sparging with O_2 (zero grade, Airgas) for at least 30 min. Titrations of NrdI in the presence of NrdF were carried out in 50 mM sodium phosphate, 20% glycerol, 200 mM NaCl, pH 7.0 (**Buffer C**) because previous characterization of NrdI had been performed in this buffer (23).

Preparation of Mn^{II}_2-NrdF

ApoNrdF (~500 μM) was expressed in *E. coli* BL21 Gold (DE3) cells (Stratagene) in the presence of 1,10-phenanthroline as previously described (32), purified to homogeneity (23), and stored in Buffer A. For most experiments, Mn^{II}_2-NrdF was prepared anaerobically by incubation of apoNrdF (330 μM) with 1.32 mM $MnCl_2$ in Buffer A. For experiments investigating the oxidation state of the dimanganese-Y• cofactor by EPR, Mn^{II}_2-NrdF (500 μL) was prepared aerobically, the excess Mn^{II} was removed by Sephadex G25 (1 × 6 cm, 5 mL), and the protein was concentrated using an Amicon Ultra 10 kDa MWCO centrifugal filtration device (Millipore) and degassed.

Preparation of $NrdI_{hq}$

N-terminally His_6-tagged NrdI (~400 μM) was purified from inclusion bodies as previously described (23) and stored in Buffer C. NrdI (500 μL) was fully reduced by titration with a 5–6 mM solution of sodium dithionite in Buffer C, in a septum-sealed anaerobic cuvette (Starna Cells) fitted with a gas-tight syringe with repeating dispenser (Hamilton) (23).

Pulldown of Mn^{II}_2-NrdF with NrdI

In a final volume of 1 mL, 12.5 μM Mn^{II}_2-NrdF and 25 μM oxidized NrdI ($NrdI_{ox}$) were mixed in Buffer B and incubated at 4 °C for 5 min before loading onto a 0.2 mL (0.7 × 1.2 cm) Ni-NTA agarose column (Qiagen). The column was washed with 6 mL Buffer B, 3 mL Buffer B containing 10 mM imidazole, 2 mL Buffer B containing 50 mM imidazole, and 1 mL Buffer B containing 250 mM imidazole. The flowthrough and column washes were collected and analyzed by SDS-PAGE. As a control, an analogous experiment was carried out with 1 mL 12.5 μM Mn^{II}_2-NrdF in Buffer B, in the absence of $NrdI_{ox}$.

Anaerobic titration of NrdI in the presence of NrdF

To a septum-sealed anaerobic cuvette fitted with a gas-tight syringe and repeating dispenser, 250 μL of apo- or Mn^{II}_2-NrdF (36 μM) and $NrdI_{ox}$ (72 μM) were added and mixed with Buffer C. The syringe contained ~1 mM sodium dithionite in Buffer C, which was added in 2 μL aliquots until no further change in the UV-vis spectrum (300 to 800 nm) occurred. Equilibrium was reached after each addition within the time required to mix the sample and to initiate spectrum acquisition.

The spectrum of the anionic semiquinone (sq) form of NrdI was estimated as previously described for the neutral sq (23). At 293 K, the visible spectrum was acquired of an anaerobic sample of 70 μM NrdI and 35 μM apoNrdF, titrated with dithionite to maximize sq formation. This sample, which now contained ox, sq, and hq forms of NrdI, was then transferred into a sealed aqueous flat cell (Wilmad) in an anaerobic box and its EPR spectrum was acquired at 293 K. Spin quantitation was performed using a Fe^{III}_2-Y• NrdF sample of known Y• concentration (see below for details). Comparison of the sq concentration, determined by EPR spectroscopy, with the visible spectrum allowed calculation of the extinction coefficient of the anionic sq at 585 nm (only $NrdI_{sq}$ has significant absorption at >550 nm), assuming that all sq was in the anionic form. The resulting value (ε_{585nm} = 1.5 mM^{-1} cm^{-1}) was used to calculate the concentration of $NrdI_{sq}$ at given points during titrations, thereby allowing determination of the concentrations of

$NrdI_{ox}$ and $NrdI_{hq}$. The spectra of $NrdI_{ox}$ and $NrdI_{hq}$ in the presence of apoNrdF, scaled by concentration, were subtracted from the overall spectrum, yielding the approximate sq spectrum.

In vitro generation of the dimanganese-Y• cofactor

In an anaerobic box, Mn^{II}_2-NrdF and variable amounts of $NrdI_{hq}$ were mixed with Buffer A (Buffer B) to give a volume of 120 μL. The reactions were initiated by addition of 130 μL O_2-saturated Buffer A (Buffer B) outside the box. The final reaction mixtures contained 10 μM (50 μM) Mn^{II}_2-NrdF, 0–20 μM (0–200 μM) $NrdI_{hq}$, and 1 mM O_2. After incubation for 1–2 min, 10 μL aliquots were frozen in liquid N_2 and subsequently assayed for activity as described below. The remainder of the solution was transferred to an EPR tube and frozen in liquid N_2 for analysis. Because NrdI is stored in Buffer C, which contains 20% glycerol, the glycerol content of the samples varied between 5 and 12%.

Removal of Mn^{II} from dimanganese-Y• NrdF

Dimanganese-Y• NrdF was prepared in a 250 μL reaction mixture containing 50 μM Mn^{II}_2-NrdF, 100 μM $NrdI_{hq}$ and 1 mM O_2, in Buffer B. After 2 min, ethylenediaminetetraacetic acid (EDTA) at a final concentration of 5 mM was added and the reaction mixture incubated at 4 °C for 2 h with gentle rocking. Mn^{II}-EDTA was removed from the protein using a Sephadex G25 column (1 × 6 cm, 5 mL), and the protein was concentrated to the original volume using an Amicon Ultra 10 kDa MWCO centrifugal filtration device and frozen in liquid N_2 for EPR analysis.

Inactivation of dimanganese-Y• NrdF by hydroxyurea (HU) and hydroxylamine

A reaction mixture of 250 μL containing 30 μM Mn^{II}_2-NrdF, 60 μM $NrdI_{hq}$, and 1 mM O_2 in Buffer B was prepared as described above. After 2 min, HU or NH_2OH was added to a final concentration of 30 mM or 1 mM and the samples were incubated at 25 °C for 20 or 5 min, respectively. The HU or NH_2OH was then removed by Sephadex G25 chromatography (1 × 6 cm, 5 mL) and the protein-containing fraction was frozen and subsequently assayed for activity.

Activity assays

A typical assay reaction contained in a final volume of 135 μL: 0.2 μM reconstituted NrdF (or NrdE), 1.0 μM NrdE (or NrdF), 0.3 mM dATP, 20 mM dithiothreitol (DTT), and 0.5 mM [^{3}H]-CDP (ViTrax, 4800–6500 cpm/nmol), in 50 mM HEPES, 15 mM $MgSO_4$, 1 mM EDTA, pH 7.6, at 37 °C (23). At four timepoints, 30 μL aliquots were removed and heated at 100 °C for 2 min. Subsequent to removal of the phosphates using alkaline phosphatase (Roche), dCDP formation was analyzed by the method of Steeper and Steuart (33). One unit (U) of activity is equivalent to 1 nmol dCDP produced/min. The SA of N-terminally His_6-tagged NrdE (23) was 80 U/mg when assayed with Fe^{III}_2-Y• NrdF (0.7 Y•/β2) or 140 U/mg when assayed with dimanganese-Y• NrdF (0.25 Y•/β2).

Reaction of dimanganese-Y• NrdF with NrdE, N_3CDP, and dATP

A reaction mixture of 240 μL contained 20 μM NrdE, 20 μM dimanganese-Y• NrdF (0.3 Y•/β2), 0.3 mM dATP, 10 mM DTT, 15 mM $MgSO_4$, and 250 μM N_3CDP (or CDP) in Buffer A. The reaction was initiated by addition of dimanganese-Y• NrdF and hand-quenched in liquid N_2 after 40 s, 1 min, or 10 min. The concentrations of the nitrogen-centered radical (N•) and Y• were determined by EPR spectroscopy at 77 K, with the N• and Y• signals deconvoluted using an in-house Excel program as described (34).

EPR spectroscopy

EPR spectra were acquired on a Brüker EMX X-band spectrometer at 77 K using a quartz finger dewar, at 3.6 to 20 K using an Oxford Instruments liquid helium cryostat, or at 293 K using an aqueous flat cell. All spectra were acquired at 9.3–9.9 GHz, 100 kHz modulation frequency. Other acquisition parameters for dimanganese-Y• NrdF were: 1) at 77 K, 1 mW power, 1.5 G modulation amplitude, 2.52×10^4 gain, 10.24 ms time constant; 2) at 20 K, 0.2 mW power, 4 G modulation amplitude, 2.52×10^4 gain, 5.12 ms time constant; and 3) at 3.6 K, 0.1 mW power, 4 G modulation amplitude, 1.26×10^4 gain, 20.48 ms time constant. Other parameters for Fe^{III}_2-Y• NrdF at 77 K were 50 μW power, 1.5 G modulation amplitude, 2.52×10^3 gain, 5.12 ms time constant. At 293 K, the parameters for $NrdI_{sq}$ were 6.3 mW power, 1.26×10^4 gain, 1.5 G modulation amplitude, 10.24 ms time constant, and for Fe^{III}_2-Y• NrdF, 8.0 mW power, 1.26×10^4 gain, 1.5 G modulation amplitude, 10.24 ms time constant (23).

a. Y• quantitation—All spectra used for spin quantitation were acquired under non-saturating conditions. At 77 K and below, spin quantitation was performed by double integration of the signal and comparison with either a $CuSO_4$ standard sample or an *Ec* NrdB sample. For NrdB, Y• content was determined by the dropline method (35) and by EPR spectroscopy at 77 K by comparison with the $CuSO_4$ standard (36). At 293 K, the standard used was a NrdF Fe^{III}_2-Y• sample whose Y• concentration had been determined at 77 K by comparison with the $CuSO_4$ standard. Analysis was carried out using WinEPR software (Brüker).

Quantitations of Y• in dimanganese-Y• NrdF were carried out at 77 K. For samples not treated by EDTA/Sephadex G25, four species were present: Y•, Mn^{II}_2 cluster, Mn^{III}_2 cluster, and mononuclear Mn^{II}. Mononuclear Mn^{II} was the predominant species other than Y• that was visible at 77 K. This Mn^{II} background signal was removed prior to Y• quantitation as follows. For the dimanganese-Y• NrdF samples prepared with various amounts of $NrdI_{hq}$ (Figure 5), the spectrum of an equal concentration of Mn^{II}_2-NrdF was acquired with identical settings. For other samples, the spectrum of an analogous dimanganese-Y• NrdF sample that had been treated with 1 mM NH_2OH to completely reduce the Y• was acquired. The background spectrum was then subtracted from the dimanganese-Y• spectrum and Y• was quantitated.

For EDTA/Sephadex G25-treated samples, which only contained Mn^{III}_2 cluster and Y•, the large linewidth of the Y• signal (~150 G) necessitated subtraction of the spectrum of a buffer sample, acquired under identical conditions, to achieve the flat baseline required for Y• quantitation.

b. Power saturation studies—The microwave power at half-saturation ($P_{1/2}$) and the inhomogeneous broadening (b) of the Y• signals were calculated by fitting the double integral of the signal per scan (I) determined at a number of spectrometer power settings (P) to equation 1 (37).

$$I = \frac{K \times \sqrt{P}}{[1+(P/P_{1/2})]^{0.5b}} \quad (1)$$

K is a sample- and instrument-dependent constant.

Preparation of Fe^{III}_2-Y• NrdF

ApoNrdF and variable amounts of ferrous ammonium sulfate were mixed anaerobically in Buffer A (227 μL total volume) and incubated for 20 min. O_2-saturated Buffer A (23 μL) was then added outside the anaerobic box to give a solution containing 50 μM apoNrdF, 0–250 μM Fe^{II}, and 175 μM O_2. A sample containing 50 μM apoNrdF, 200 μM Fe^{II}, 100 μM $NrdI_{hq}$, and 175 μM O_2 was also prepared analogously in Buffer B. After 1–2 min, a 10 μL aliquot was removed from each reaction and frozen for subsequent activity assays, and the remainder of the mixture was transferred to an EPR tube and frozen in liquid N_2 for analysis.

Efforts to determine the oxidant generated by reaction of $NrdI_{hq}$ with O_2

Several experiments were carried out to look for evidence for production of $O_2^{\bullet-}$ by reaction of $NrdI_{hq}$ with O_2 and for cluster assembly in Mn^{II}_2-NrdF with H_2O_2 or $O_2^{\bullet-}$. The results were negative, and these experiments are described in the Supporting Information (SI).

RESULTS

Attempts to self-assemble active dimanganese-Y• cofactor in the absence of NrdI

Previous attempts to self-assemble an active dimanganese cofactor in vitro starting with *St* Mn^{II}_2-NrdF by addition of O_2 or with *Ca* Mn^{II}_2-NrdF by addition of O_2 or H_2O_2 failed to generate any significant Y• or activity (11). We also attempted self-assembly experiments with *E. coli* apoNrdF. ApoNrdF was obtained by its overexpression in the presence of 1,10-phenanthroline in the growth medium (23, 32). The isolated protein contained 0.01 Mn/β2, assayed by atomic absorption spectroscopy, and 0.03 Fe/β2, using the ferrozine assay. Activity assays revealed no detectable dCDP formation.

ApoNrdF was then mixed anaerobically with 4 Mn^{II}/β2 and the EPR spectrum of the resulting material was recorded at 20 K (Figure 1). The EPR signal, displaying an average effective nuclear hyperfine coupling constant (a_{Mn}) of 46 G, is consistent with two weakly antiferromagnetically coupled Mn^{II} ions and is similar to the spectra previously reported for the *Ca* and *St* Mn^{II}_2-NrdFs (11) and the Mn^{II}_2-catalases (38, 39). Mn^{II}_2-NrdF was then exposed to either an excess of O_2 or 4 H_2O_2/β2 at 25 °C for 20 min. The visible spectra of the resulting mixtures exhibited no absorption features consistent with Y• and an assay of the reaction mixtures for dCDP formation revealed a SA of 5 U/mg in each case. The results suggest that, as with the *St* and *Ca* enzymes, *Ec* Mn^{II}_2-NrdF is unable to assemble a significant amount of an active dimanganese-Y• cofactor with the physiological oxidants O_2 and H_2O_2.

NrdI interacts with NrdF in vitro and in vivo

a. Evidence from Ni affinity chromatography—Our previous results that $NrdI_{hq}$ can specifically reduce met-NrdF (diferric NrdF with the Y• reduced) to the diferrous form (23) suggested a direct interaction between NrdF and $NrdI_{hq}$ in vitro. This interaction was confirmed by Ni affinity chromatography of a mixture of untagged Mn^{II}_2-NrdF and 2 His_6-tagged $NrdI_{ox}$/β2 (Figure 2, lanes 1–5). The mixture was loaded onto a Ni affinity column (lane 1) and washed extensively with Buffer B containing 0 mM [30 column volumes (CV), lane 2], 10 mM (15 CV, lane 3), and 50 mM imidazole (10 CV, lane 4), before elution with 5 CV Buffer B containing 250 mM imidazole (lane 5). The fractions were analyzed by 17% SDS-PAGE. Approximately 45% of the total NrdF, quantified by densitometry, coeluted with NrdI at 250 mM imidazole. By contrast, in a control experiment (lanes 6–8), Mn^{II}_2-NrdF in the absence of NrdI eluted completely by the end of the 30 CV Buffer B wash. These results demonstrate a tight interaction between $NrdI_{ox}$ and Mn^{II}_2-NrdF.

b. Evidence from perturbations of the visible spectrum of NrdI—The sensitivity of flavins to their environment suggested that the spectrum of NrdI's FMN cofactor in different oxidation states might serve as a probe for its interaction with NrdF. Incubation of $NrdI_{ox}$ or $NrdI_{hq}$ with 1 eq apoNrdF demonstrated slight perturbations of the flavin spectrum relative to the control in the absence of apoNrdF, primarily in the 350–410 nm region (Figure 3, solid and dashed lines). Our previous studies had shown that anaerobic titration of $NrdI_{ox}$ with dithionite in the absence of NrdF led to stabilization of a maximum of 28% of total flavin as a neutral sq intermediate (Figure 3, red dotted line) (23). A similar titration carried out in the presence of apoNrdF (Figure S1A) gave a surprising result. The spectrum of the one-electron reduced species (Figure 3, black dotted line, deconvoluted as described in Materials and Methods) revealed the presence of an anionic sq. Comparison of this spectrum to that of the neutral sq demonstrates striking differences, especially in the 350–410 and 550–700 nm regions. The amount of NrdI anionic sq stabilized (31–34%), determined by EPR spectroscopy, was similar to the amount of neutral sq stabilized in the absence of apoNrdF, suggesting that the ox/sq and sq/hq equilibria were not greatly altered. Titrations carried out with Mn^{II}_2-NrdF in place of apoNrdF gave similar results. Therefore, binding of NrdI to NrdF affects the environment of the flavin in all three of its oxidation states, illustrated most clearly by the altered protonation state of the sq. NrdI's formation of anionic sq in the presence of NrdF is reminiscent of flavoprotein oxidases, which react rapidly with O_2 to form H_2O_2, as opposed to flavodoxins, which stabilize neutral sq and react with O_2 to form $O_2^{\bullet-}$ (27). This analogy suggests that NrdI's function in the class Ib RNR system may be different than the electron transfer role we have proposed previously (23).

Finally, when an N-terminally StrepII-tagged NrdF was expressed in the *E. coli* strain GR536, grown in extreme Fe limitation with Mn added to the growth medium, SDS-PAGE analysis of the purified NrdF also revealed a protein of 15 kDa, consistent with the presence of NrdI (data not shown). The UV-vis spectrum of the purified NrdF suggested the presence of an oxidized flavin (5–10% of NrdF concentration, similar to the SDS-PAGE result), supporting the assignment of the co-purifying protein as NrdI. Thus, results in vitro and in vivo support strong interaction between NrdI and NrdF.

In vitro assembly of an active dimanganese-Y• cofactor in NrdF

Our inability to obtain significant activity in Mn^{II}_2-NrdF with O_2 or H_2O_2 and our in vitro and in vivo evidence for interaction between NrdF and NrdI suggested a role for NrdI in cluster assembly. We hypothesized that $NrdI_{hq}$ in the presence of O_2 could generate an oxidant (H_2O_2, HO_2^-, or $O_2^{\bullet-}$) that could be delivered directly to the Mn^{II}_2 center in NrdF and be required to assemble active cofactor. The failure of reconstitutions in the absence of NrdI might then be explained by NrdI binding to Mn^{II}_2-NrdF and affecting its structure and/or reduction potential (if H_2O_2 is the oxidant), or by forming an oxidant not tested previously (HO_2^- or $O_2^{\bullet-}$).

Mn^{II}_2-NrdF (50 μM dimer) was incubated anaerobically with $NrdI_{hq}$ (100 μM monomer) in Buffer B. Exposure of the sample to O_2 (1 mM) resulted in rapid generation of $NrdI_{ox}$ and a sharp absorption feature at 408 nm consistent with a Y• (Figure 4A, solid line and inset). The SA of the resulting protein was 600 U/mg. No loss of activity was observed after 20 min incubation at room temperature. Control experiments indicated that no Y• or activity was generated when O_2 was added to $NrdI_{hq}$ prior to its mixing with Mn^{II}_2-NrdF (Figure 4A, dashed line) or to apoNrdF preincubated with $NrdI_{hq}$. Thus, $NrdI_{hq}$ plays a key role in generating active dimanganese-Y• NrdF in the presence of O_2.

Subtraction of the spectrum of Mn^{II}_2-NrdF in the presence of 2 $NrdI_{ox}$/β2 from that of dimanganese-Y• NrdF (Figure 4B) reveals, in addition to the Y• (Figure 4A, inset), a trailing

absorbance feature. This feature is suggestive of an oxidized, μ-oxo-bridged dimanganese cluster, given the known spectra of the Mn^{III}_2 and $Mn^{IV}Mn^{III}$ forms of Mn catalases (40, 41).

Correlation of Y• and activity of the dimanganese-Y• cofactor

Studies of class Ia NrdBs have demonstrated that their SA is directly correlated with their Y• content. To determine if a similar correlation is observed with the dimanganese-Y• cofactor, Mn^{II}_2-NrdF was incubated with increasing amounts of $NrdI_{hq}$ in Buffer B and then exposed to O_2. The rate of dCDP formation and the Y• content were then measured for each sample. The results are shown in Figure 5A. Y•/β2 and SA increased with increasing amounts of NrdI up to 1–1.5 NrdI/β2, with a maximum of 0.25 Y•/β2 formed and 600 U/mg SA. A similar experiment carried out in Buffer A gave a maximum SA of 800 U/mg, but $NrdI_{hq}$ is not sufficiently soluble in this buffer to carry out the EPR experiment to quantitate Y•. ApoNrdF contains only 0.03 Fe/β2, which if completely organized in diferric-Y• cofactor would contribute at most 10 U/mg SA, based on the 500 U/mg/Y• SA calculated for diferric-Y• NrdF (see below). These data strongly suggest that the cofactor formed in these experiments contains Mn and Y•.

As shown in Figure 5B, SA/Y• appears to decrease with increasing Y•/β2. We suggest that this result is due to the low SA of our NrdE (α2) preparations [80 or 140 U/mg, depending on the metallocofactor, vs. 280 U/mg for *St* NrdE with Fe^{III}_2-Y• NrdF (12)], which in turn limits NrdF activity.

To provide additional support for the importance of Y• for catalytic activity, dimanganese-Y• NrdF was incubated with hydroxyurea (HU) and hydroxylamine. HU reduces Y• without affecting the diferric clusters of bacterial β2s such as *Ec* NrdB (42) and *Ec* (23) and *Ba* (43) Fe^{III}_2-Y• NrdFs, but it reduces both Y• and diferric cluster in the case of mouse β2 (44). NH_2OH reduces the Y• of *Ba* Fe^{III}_2-Y• NrdF (43) and *Ec* NrdB (45); in the latter case at least it also reduces diferric cluster. NH_2OH is also known to reduce the Mn^{III}_2 and $Mn^{IV}Mn^{III}$ forms of Mn catalases (46). When NH_2OH (1 mM) was incubated with 30 μM dimanganese-Y• NrdF at 25 °C, the visible features of Y• were abolished within 1 min. On the other hand, HU, even at 30 mM, required 10 min for Y• reduction under the same conditions. Both samples retained activity, 96 and 56 U/mg, respectively, which correlates with <0.05 Y•/β2, difficult to detect by vis spectroscopy. The residual activity after HU or NH_2OH treatment cannot correspond to diferric-Y• cofactor, which is known to be efficiently reduced by these reagents on this timescale.[2] A control in the absence of HU or NH_2OH retained full activity at the end of the incubation. These data support the importance of the Y• for activity.

It was also observed that Y• reduction by HU and NH_2OH was accompanied by a slower decrease in the intensity of the trailing absorption feature that we have suggested is associated with an oxidized Mn cluster in dimanganese-Y• NrdF (Figure 4B, 400–700 nm). In the case of NH_2OH, a 40% decrease was apparent within 1 min, whereas in the case of HU, no decrease was apparent in the first minute but a 30% decrease was visible within 5 min. After these initial declines, little further decrease was observed over 5 min. These results, suggestive of reduction of oxidized Mn cluster by both HU and NH_2OH, are consistent with observations that NH_2OH can reduce the $Mn^{IV}Mn^{III}$ and Mn^{III}_2 forms of Mn catalases (46). A more detailed analysis of the effects of HU and NH_2OH on Y• and

[2]A reviewer suggested that the residual activity after HU and NH_2OH treatment may be due to a small amount of a Y•-independent cofactor, such as $Mn^{IV}Fe^{III}$, which has been identified in the *Chlamydia trachomatis* class Ic RNR (56). We do not favor this option because we have observed no evidence for an EPR-active $Mn^{III}Fe^{III}$ species upon incubation of Mn^{III}_2-Y• NrdF with N_3CDP, NrdE, and dATP (see below). However, we cannot completely rule out the possibility of a small amount of $Mn^{IV}Fe^{III}$ species at present.

dimanganese cluster will be carried out once more homogeneous dimanganese-Y• cofactor is obtained.

The active cofactor is Mn^{III}_2-Y•

The oxidation state of the Mn center in active dimanganese-Y• NrdF was investigated by EPR spectroscopy at 20 and 3.6 K, as the EPR features of the cluster are poorly defined at liquid N_2 temperatures and above. The EPR spectrum at 20 K of a representative sample prepared with 2 $NrdI_{hq}$/β2 in Buffer B (Figure 6A, black line), with 3.4 ± 0.2 Mn/β2 and 0.25 ± 0.03 Y•/β2, shows a sharp feature at g = 2.0054 associated with Y•, as well as lesser amounts of the Mn^{II}_2 cluster signal relative to a Mn^{II}_2-NrdF sample in the presence of $NrdI_{ox}$ (Figure 6A, red line). The spectrum of the Mn^{II}_2 cluster is broad and a baseline could not be obtained. Therefore, for comparison of the relative amounts of Mn^{II}_2 cluster between the two samples, the peak-to-trough intensity (47) of the most intense Mn^{II}_2-NrdF hyperfine line was used (Figure 6A, arrows). This amplitude was reduced by 45% in dimanganese-Y• NrdF generated with 2 $NrdI_{hq}$/β2, relative to the Mn^{II}_2-NrdF and $NrdI_{ox}$ control (Figure 6A, inset). Since NrdF contains 3.4 Mn/β2 (1.7 dimanganese clusters/β2), these results suggest formation of 0.8 oxidized Mn cluster/β2.

Mn^{III}_2, $Mn^{II}Mn^{III}$, and $Mn^{IV}Mn^{III}$ clusters were considered as possible components of the active dimanganese-Y• cofactor in NrdF. Previous studies of Mn catalases (40) and model complexes mimicking Mn catalases (48) have revealed the rich EPR spectra associated with $Mn^{II}Mn^{III}$ and $Mn^{IV}Mn^{III}$ clusters and optimized temperature and power settings for cluster detection (38, 40, 49). However, extensive analysis (see SI) failed to reveal the characteristic features of these clusters. Thus the most likely oxidation state of the active metallocofactor is Mn^{III}_2, which would be EPR-silent if antiferromagnetically coupled.

In order to obtain further evidence in support of this proposal, dimanganese-Y• NrdF was treated with EDTA, in an effort to remove Mn^{II} from NrdF. Following removal of Mn^{II}-EDTA by Sephadex G25 chromatography, NrdF retained 1.4 ± 0.2 Mn/β2, consistent with the above calculation of 0.8 oxidized clusters/β2. EPR spectra of the resulting protein at 20 K demonstrated complete removal of the Mn^{II}_2 cluster features (Figure 6B), while the Y• content of the protein was unaffected (0.28 ± 0.01 Y•/β2). This analysis suggests Mn^{III}_2-Y• is the NrdF cofactor. However, the possibility of a $Mn^{II}Mn^{III}$ or $Mn^{IV}Mn^{III}$ cluster, strongly antiferromagnetically coupled to a population of Y• such that both metal cluster and Y• are EPR silent, cannot be excluded on the basis of these experiments alone.

Confirmation of the identity and activity of the Mn^{III}_2-Y• cofactor using N_3CDP

The mechanism-based inhibitor 2′-azido-2′-deoxycytidine 5′-diphosphate (N_3CDP) was employed to confirm the importance of the Y• in NrdF in deoxynucleotide formation and to rule out the presence of an exchange-coupled $Mn^{II}Mn^{III}$-Y• or $Mn^{IV}Mn^{III}$-Y• cofactor. Previous studies have shown that class Ia RNRs are inactivated by 2′-azido-2′-deoxynucleoside diphosphates, accompanied by rapid loss of ~50% Y• (<30 s) and formation of ~50% of a new nitrogen-centered radical (N•) in α2 (50, 51), and that after 20 min, ~90% Y• is reduced (50). Detection of N• thus indicates that RNR is active in nucleotide reduction. Similar experiments have not been reported for a class Ib RNR. To provide additional support for the activity of Mn^{III}_2-Y• NrdF, the protein was incubated with NrdE, allosteric effector dATP, and N_3CDP. The reaction was quenched after 40 s and the spin quantitated by EPR spectroscopy at 77 K. Under these conditions, the total radical concentration remained unchanged and 60% of the total spin was found to be associated with N• and 40% with Y• (all values ± 10%). When the reaction was quenched after 10 min, 25% of the initial spin was lost, with 20% of the remaining spin as Y• and 80% as N•. Given that a control without N_3CDP retains the same amount of total radical over the course of this

10 min incubation, at least 80% of the total Y• is active. These studies also rule out the presence of mixed-valent Mn clusters antiferromagnetically coupled to Y•, as no new EPR signals, other than N•, are detected. Therefore, the data together support Mn^{III}_2-Y• as the active cofactor in NrdF.

Y• interacts with the Mn^{III}_2 cluster

The EPR spectra of Mn^{III}_2-Y• NrdF and Fe^{III}_2-Y• NrdF (see below for preparation of the latter) at 77 K are shown in Figure 6C (black and red lines, respectively). The former signal has a larger linewidth (~150 G vs. 60 G for diferric Y•) and the hyperfine features associated with the β and ring hydrogens are more poorly resolved than for the Fe^{III}_2-Y•. At 20 K, however, additional, lower intensity features (between 3100–3600 G) are present to the low- and high-field sides of the "sharp" signal, 150 G in width (Figure 6B). These "broader" features at 20 K become more prominent at 3.6 K (Figures 6D). However, we were unable to obtain a completely flat baseline at this temperature (Figure S3), possibly suggesting the presence of an additional EPR-active species. The EPR features between 3100 and 3600 G are not present in Fe^{III}_2-Y• NrdF or in Mn^{II}_2-NrdF in the presence of $NrdI_{ox}$. They are also absent in Mn^{III}_2-Y• NrdF treated with NH_2OH or HU and are decreased upon N_3CDP treatment, demonstrating that these features are associated with Y•.

Relaxation properties of the Y•

The microwave power at half-saturation ($P_{1/2}$) values of Y• in Mn^{III}_2-Y• NrdF at 3.6 and 77 K were measured (Table 1) and found to be two orders of magnitude higher than for *E. coli* and other Fe^{III}_2-Y• NrdFs. The strong temperature dependence of the spectra (Figure 6B–D) and faster relaxation of the Y• at 3.6–77 K relative to the Fe^{III}_2-Y• cluster may reflect a smaller magnitude of the exchange coupling constant (J) for the Mn^{III}_2 cluster relative to the Fe^{III}_2 cluster. This would result in greater population of paramagnetic excited states of the antiferromagnetically coupled Mn^{III}_2 cluster, leading to faster relaxation of Y•. Alternatively, the data could also reflect the Mn^{III}_2 cluster being ferromagnetically coupled, such as with an $S = 4$ ground state. Studies are in progress to further characterize the electronic properties of the Mn^{III}_2-Y• cofactor to evaluate these proposals.

Fe^{III}_2-Y• cofactor assembly in the absence and presence of $NrdI_{hq}$

Because Fe^{III}_2-Y• cofactor can self-assemble from Fe^{II}, O_2, and apoNrdF, a systematic investigation of whether SA correlates with Y• in Fe^{III}_2-Y• NrdF was also carried out to compare with our Mn^{III}_2-Y• cofactor results. ApoNrdF was incubated anaerobically with 0, 0.6, 1, 2, 3, 4, or 5 Fe^{II}/β2 and exposed to 3.5 O_2/β2, the Y• was quantitated by EPR, and the resulting protein was assayed for dCDP formation. The highest Y• content achieved was 0.7 Y•/β2, with an activity of ~300 U/mg (Figure 7A). However, as was observed with Mn^{III}_2-Y• NrdF, the SA/Y• also decreases as Y• increases (Figure 7B). While the maximum Y• content of Fe^{III}_2-Y• NrdF is higher than for Mn^{III}_2-Y• NrdF, the SA/Y• is 4 times higher for Mn^{III}_2-Y• NrdF.

The ability to form Fe^{III}_2-Y• NrdF in the presence of $NrdI_{hq}$ under conditions analogous to those described for the Mn^{III}_2-Y• cofactor was also investigated. Y• content similar to that observed with Mn^{III}_2-Y• NrdF resulted (0.19 Y•/β2), but the SA was only 78 U/mg. This SA per Y• (~500 U/mg/Y•) is similar to that observed when NrdF is reconstituted with 4 Fe^{II}/β2 and O_2 alone, but only ~1/3 the amount of Y• was generated. Thus, while $NrdI_{hq}$ is required for Mn^{III}_2-Y• cofactor assembly, it appears to interfere with Fe^{III}_2-Y• cofactor assembly in vitro.

DISCUSSION

Formation of a Mn^{III}_2-Y• cofactor

Despite the documented dependence of *C. ammoniagenes* and other gram-positive bacteria on Mn^{II} for growth, DNA synthesis, and possibly deoxynucleotide formation (8, 17), general acceptance of the proposal by Follmann, Auling, and coworkers of a Mn-containing class Ib RNR in these organisms (10) has been hindered by the inability to assemble active Mn-containing cofactor in vitro and the low activity of the purified *Ca* NrdF (11, 13). In this work, we have demonstrated for the first time that a Mn^{II}_2-NrdF is competent in vitro to form an active Mn^{III}_2-Y• cofactor in the presence of $NrdI_{hq}$ and O_2.

Our assignment of Mn^{III}_2-Y• as the active form of NrdF is supported by previous experiments with *Ca* NrdF. The visible spectrum of that protein, reported by Follmann, Auling, and coworkers (10), is similar to that of μ-oxo, di-μ-carboxylato-Mn^{III}_2 model compounds synthesized by the Wieghardt (52) and Lippard (53) groups. However, our demonstration that NrdI copurifies with NrdF suggests that certain features of the *Ca* NrdF visible spectrum could have been associated with NrdI. When *Ca* NrdF was purified by Sjöberg and coworkers (13), it contained 1 Mn/β2 and was EPR silent. This observation is also consistent with the presence of a Mn^{III}_2 cluster. No Y• was detected by either the Auling or the Sjöberg group, although HU was able to abolish the low levels of activity, suggesting its presence. In neither case was the yield of active enzyme sufficiently high for biophysical characterization. We propose that we have formed in vitro the same NrdF cofactor isolated from *C. ammoniagenes*, and perhaps more recently from *Corynebacterium glutamicum* (14).

The role of NrdI in Mn^{III}_2-Y• cofactor assembly

Reaction of $NrdI_{hq}$ with O_2 could potentially generate $O_2^{\bullet-}$, H_2O_2, or HO_2^-, which are all potential oxidants of Mn^{II}_2-NrdF. A number of experiments were carried out in an effort to identify the oxidant (see SI). Our efforts to form active cofactor from Mn^{II}_2-NrdF using $O_2^{\bullet-}$ generated aerobically by the xanthine/xanthine oxidase system, in the presence or absence of $NrdI_{ox}$, have been unsuccessful. We have also looked for $O_2^{\bullet-}$ formation using the nitrone spin trap 5-(diethoxyphosporyl)-5-methyl-1-pyrroline *N*-oxide (DEPMPO) by incubation of $NrdI_{hq}$, apoNrdF, and O_2. While very low levels of $O_2^{\bullet-}$ were trapped, the amounts were insufficient to account for the 0.25 Y•/β2 we have observed in Mn^{III}_2-Y• NrdF. Thus $O_2^{\bullet-}$ does not appear to be the oxidant involved in Mn^{III}_2-Y• cofactor assembly.

Cluster assembly aerobically using H_2O_2 as oxidant, in the presence or absence of $NrdI_{ox}$, gave a SA of 5 U/mg. Interestingly, when Mn^{II}_2-NrdF was exposed to a five-fold excess of H_2O_2 over 20 min under anaerobic conditions in the presence of $NrdI_{hq}$ (SI), a significant amount of active cofactor (330 U/mg) was generated. However, $NrdI_{hq}$ was fully oxidized in both this experiment and a control reaction containing apoNrdF in place of Mn^{II}_2-NrdF. This result suggests that generation of active cofactor was not associated with H_2O_2 reacting with Mn^{II}_2-NrdF, but instead with catalase activity unrelated to the manganese cluster that generated O_2, which in turn reacted with $NrdI_{hq}$ to form Mn^{III}_2-Y• cofactor.

An alternative oxidant such as ClO^- could be generated from buffer components. However, removal of Cl^- from Buffer C and use of $MnSO_4$ in place of $MnCl_2$ did not significantly affect the SA of the reconstituted Mn^{III}_2-Y• NrdF.

Based on these negative results, our working model is that $NrdI_{hq}$ reacts with O_2 to produce HO_2^-, although we cannot completely rule out H_2O_2 production. The oxidant is then channeled to Mn_B (the Mn farthest from the Y to be oxidized) in NrdF via a hydrophobic channel from the protein surface; this channel has been suggested to be the route of O_2

access to the metal cluster in other class I RNRs (20, 54, 55). Channeling of the oxidant to the metal site is supported by the observation that Mn^{III}_2-Y• NrdF assembly is not affected by the presence of superoxide dismutase (SOD) or catalase (see SI). If this proposal is correct, NrdI is acting more like a flavoprotein oxidase than a flavodoxin. The use of H_2O_2 as an oxidant to efficiently generate an active RNR cofactor has been demonstrated in studies on the *Chlamydia trachomatis* class Ic RNR, which uses an active $Mn^{IV}Fe^{III}$ cofactor, not Y•, in catalysis (56). In that system, H_2O_2 can function in vitro to generate quantitatively the active $Mn^{IV}Fe^{III}$ cofactor from either the $Mn^{II}Fe^{II}$ or $Mn^{III}Fe^{III}$ forms of the protein (57).

Proposed mechanism of Mn^{III}_2-Y• cofactor formation (Scheme 1)

Because the Mn^{II}_2 center of NrdF is not reactive with O_2, we propose that NrdI must convert two molecules of O_2 to HO_2^- to access the metal cluster oxidation states high enough to oxidize Y_{105} to Y•. Our working model for this process is shown in Scheme 1. We suggest that the first steps in Mn^{III}_2-Y• cofactor formation in NrdF are analogous to those proposed for the reaction of reduced Mn catalase with H_2O_2 (58, 59). Mn catalases catalyze the disproportionation of H_2O_2 to O_2 and H_2O in an active site that cycles between the Mn^{II}_2 and Mn^{III}_2 states (47). Furthermore, the active sites of the Mn catalases share important structural features with O_2-activating diiron enzymes like the class Ia RNRs, methane monooxygenase, and Δ^9 desaturase (60, 61). For these reasons, Mn catalases have served as a framework for the first step (Scheme 1, A) of Mn^{III}_2-Y• cofactor assembly in NrdF.

In step A (Scheme 1), NrdF-bound $NrdI_{hq}$ is proposed to reduce O_2 to HO_2^-, which channels to the metal site and initially binds terminally to Mn_B^{II}. Binding to the B site is proposed based on crystal structures of N_3^- bound to class Ia RNRs (62) and Mn catalase (61). Reorganization of the hydroperoxide ligand, protonation, and heterolytic O-O bond cleavage could lead to a μ-oxo-bridged Mn^{III}_2 cluster as proposed for Mn catalases (58, 63).

The reduction potentials of dimanganese(III) model complexes (52, 53, 63, 64) are unlikely to be high enough to oxidize Y_{105} to Y• [$E_{Y•/Y}$ ~1.2 V vs. NHE (65)]; therefore, a second equivalent of HO_2^- must be provided by NrdI to generate the Y• (step B, Scheme 1). $NrdI_{ox}$ must either dissociate from NrdF to allow binding of a second $NrdI_{hq}$ or be reduced by an unknown reductant. Our preliminary in vitro evidence for a tight interaction between NrdI and NrdF suggests that the latter is the case in vivo. Following the second reaction of $NrdI_{hq}$ with O_2, a second HO_2^- is proposed to bind to Mn_B. Here the analogy to the Mn catalases ends, as HO_2^- oxidizes rather than reduces the Mn^{III}_2 cluster. The reduction potentials of the $Mn^{IV}Mn^{III}$ to Mn^{III}_2 couples of μ-oxo, μ-carboxylato-bridged dimanganese model complexes have been reported to fall in the 0.7–0.9 V range (52, 53). Reduction potentials of Mn^{IV}_2 to $Mn^{IV}Mn^{III}$ couples of these complexes are so high [e.g. 1.6 V (53)] that oxidation of $Mn^{IV}Mn^{III}$ complexes that contain phenolate ligands has been reported to lead to oxidation of the ligand to the phenoxyl radical instead of oxidation to the Mn^{IV}_2 state (66). We suggest that in NrdF, oxidation of the Mn^{III}_2 cluster by the bound hydroperoxide does not lead to Mn^{IV}_2 formation; rather, W_{31} is oxidized, leading to a di-μ-oxo-$Mn^{IV}Mn^{III}$–$W_{31}^{+•}$ intermediate. The $W_{31}^{+•}$ would then be reduced by an exogenous reductant. This aspect of our mechanism parallels the self-assembly pathway of the class Ia RNR's Fe^{III}_2-Y• cofactor, in which a μ-1,2-peroxodiferric intermediate (67) is reduced by W_{48} (*Ec* NrdB numbering) to form a μ-oxo-bridged $Fe^{IV}Fe^{III}$ intermediate (**X**), rather than an Fe^{IV}_2 species (68–70). **X** subsequently oxidizes Y_{122} to the Fe^{III}_2-Y• cofactor (71). Likewise, the reduction potential of the $Mn^{IV}Mn^{III}$ species in NrdF is expected to be in the range to be able to oxidize Y_{105}, resulting in the Mn^{III}_2-Y• cofactor.

Substoichiometry of Y• formation in NrdF

Our efforts so far to increase Y• content in Mn^{III}_2-Y• NrdF have been unsuccessful.[3] The complexity of the mechanistic proposal in Scheme 1, however, provides a rationalization for our lack of success. Specifically, in our in vitro reconstitutions, after NrdF-bound $NrdI_{hq}$ reacts with O_2 to form HO_2^- and Mn^{III}_2-NrdF, it must be reduced by another $NrdI_{hq}$ in solution. This is expected to be an inefficient process due to disproportionation of the ox and hq forms to form sq. Alternatively, orchestration of the sequential binding of two $NrdI_{hq}$s to NrdF with the appropriate timing would also be challenging. These gymnastics could be avoided in vivo with a physiological reductant. NrdI could then act catalytically.

We also investigated whether $NrdI_{hq}$ could reduce the Y• of Mn^{III}_2-Y• cofactor, thereby contributing to the substoichiometric Y• content (see SI). We found that, although Y• content was reduced from 0.3 to 0.2 Y•/β2 over 30 min, this reduction is likely too slow to contribute significantly in the cluster assembly reactions, which are complete within seconds. We therefore favor the absence of the putative NrdI reductase as the explanation for substoichiometric Mn^{III}_2-Y• cofactor assembly in our in vitro reconstitutions. We are currently using a bioinformatic approach to identify this protein.

Implications for the maintenance pathway

The requirement for 2 eq HO_2^- in cluster assembly also requires that the $NrdI_{hq}$ bound to Mn^{III}_2-NrdF must not reduce the manganese cluster before $NrdI_{hq}$ reacts with O_2. However, we have previously shown that $NrdI_{hq}$ efficiently reduces met-NrdF to Fe^{II}_2-NrdF, and we proposed that this maintenance role may be operative in vivo. A similar maintenance function for NrdI, in addition to its biosynthetic role, may also exist for Y•-reduced Mn^{III}_2-NrdF. In this case, $NrdI_{hq}$ would be involved in step B (Scheme 1), to reoxidize the Y to the Y•. In preliminary experiments in which EDTA-treated, Y•-reduced Mn^{III}_2-NrdF was incubated anaerobically with $NrdI_{hq}$, formation of at least 80% Mn^{II}_2 cluster was observed by EPR. Therefore, $NrdI_{hq}$ can reduce Mn^{III}_2-NrdF, at least within the 4 min required for these samples' preparation. However, it is possible that this process is slow enough not to compete with reaction of $NrdI_{hq}$ with O_2 in vivo. Further studies are in progress to determine the relative kinetics of oxidation of $NrdI_{hq}$ by Mn^{III}_2-NrdF versus by O_2.

Is the Mn^{III}_2-Y• cofactor active in vivo?

The remarkable observation that *Ec* NrdF is active in nucleotide reduction in vitro with both Fe^{III}_2-Y• and Mn^{III}_2-Y• cofactors could mean that both forms are physiologically relevant. For example, *E. coli* contains Fe-dependent and Mn-dependent SODs, with the latter being upregulated in Fe-limited growth conditions (72). In addition, certain, so-called "cambialistic," SODs are active in both Fe and Mn forms. The *Propionibacterium shermanii* cambialistic SOD purifies with Fe when the organism is grown in rich media but purifies with Mn when grown under Fe-limited conditions in the presence of Mn^{II} (73). Imlay and coworkers have proposed that in *E. coli*, metallation of certain enzymes may be flexible; for example, those enzymes may use Fe^{II} when grown in the absence of oxidative stress and Mn^{II} under oxidative stress conditions, to avoid protein and cell damage (19). Likewise, it is possible that Fe^{III}_2-Y• NrdF is active in Fe-replete conditions, while Mn^{III}_2-Y• NrdF will be active in Fe-limited conditions and will require NrdI for assembly.

[3]We have attempted to express NrdF under a variety of conditions: 1) using 2 mM $MnCl_2$ in the growth medium (11) in the presence of 100 μM 1,10-phenanthroline (32) to chelate iron; 2) controlling the levels of expression with arabinose by placing *nrdF* in a pBAD vector; and 3) coexpressing the entire *nrdHIEF* operon. We have also investigated a number of self-assembly protocols, including: 1) removal of NrdI's N-terminal His tag; 2) removal of Cl^- (present in Buffer C and therefore also in the assembly reactions), as it has been shown bind to and inhibit the Mn^{II}_2 form of *Thermus thermophilus* Mn catalase (38); 3) addition of ascorbate as a source of a reducing equivalent (69); 4) addition of NrdE; 5) cluster assembly in 50 mM MOPS and Tris buffers, pH 7.6; and 6) cluster assembly with smaller amounts of O_2 added. None of these methods led to increased SA of NrdF or increased Y•.

Studies of Rensing and coworkers have demonstrated that growth of *E. coli* GR536, a strain deficient in all known iron uptake systems, is dependent on Mn under severely Fe-limited conditions (18). Preliminary studies in our laboratory (Cotruvo and Stubbe, unpublished results) have shown that NrdF is expressed in these conditions and the purified protein is active in nucleotide reduction and contains Mn. NrdF expressed under Fe limitation and oxidative stress is thus likely to contain a Mn^{III}_2-Y• cofactor in *E. coli*.

In other organisms that depend on the class Ib RNR for DNA replication in aerobic growth, it is possible that both diiron and dimanganese cofactors are used in vivo, depending on the growth conditions. Several observations suggest, however, that in these organisms as well, the Mn^{III}_2-Y• cofactor may be active. First, studies in *C. ammoniagenes* (8, 17) have suggested that Mn is required for growth and possibly deoxynucleotide formation. Isolation of a Mn-containing NrdF, with only trace amounts of Fe, from this organism (10, 13), even when cells were grown in Fe-containing media (15), argues for Mn being present in *Ca* NrdF in a variety of growth conditions. Furthermore, the ubiquitous presence of *nrdI* contiguous to *nrdEF*, suggesting coordinated expression, implies that NrdI plays an essential role in all class Ib RNRs in vivo, such as in metallocofactor biosynthesis. While we have found that NrdI is required for Mn^{III}_2-Y• cofactor generation in NrdF, it is not required and in fact hinders Fe^{III}_2-Y• cofactor formation in NrdF in vitro.

Therefore, our current hypothesis is that NrdF contains the Mn^{III}_2-Y• cofactor in *E. coli* and related enterobacteria, whereas the identity of the cofactor in other organisms containing class Ib RNRs may depend on the specific organism and/or growth conditions. We are working to establish the metal requirements of NrdF proteins under a variety of growth conditions in several prokaryotes by integrating N-terminally tagged *nrdF*s into genomes for expression at endogenous levels.

The in vitro activity of both Mn^{III}_2-Y• and Fe^{III}_2-Y• cofactors in NrdF underscores the importance of the cellular metallocofactor assembly machinery (e.g. chaperone proteins, metal transporters, and deliverers of reducing equivalents), which may not be available when metalloproteins are expressed heterologously in rich media. In vivo studies must accompany in vitro studies, to ensure the metalloenzymes being examined in molecular detail are physiologically relevant.

Supplementary Material

Refer to Web version on PubMed Central for supplementary material.

Acknowledgments

We thank Prof. Stephen Lippard (MIT) for use of his laboratory's atomic absorption spectrometer and Justin Wilson for assistance in data acquisition, and Christopher Rensing (University of Arizona) for the generous gift of *E. coli* GR536. We also thank Prof. Lippard, Prof. James Imlay (University of Illinois at Urbana-Champaign), and members of the Stubbe laboratory, especially Ellen Minnihan and Kenichi Yokoyama, for valuable discussion. We are also indebted to Ellen Minnihan for synthesizing the N_3CDP used in these studies.

References

1. Nordlund P, Reichard P. Ribonucleotide reductases. Annu Rev Biochem. 2006; 75:681–706. [PubMed: 16756507]
2. Uppsten M, Farnegardh M, Jordan A, Eliasson R, Eklund H, Uhlin U. Structure of the large subunit of class Ib ribonucleotide reductase from *Salmonella typhimurium* and its complexes with allosteric effectors. J Mol Biol. 2003; 330:87–97. [PubMed: 12818204]

3. McHugh JP, Rodriguez-Quiñones F, Abdul-Tehrani H, Svistunenko DA, Poole RK, Cooper CE, Andrews SC. Global iron-dependent gene regulation in *Escherichia coli* A new mechanism for iron homeostasis. J Biol Chem. 2003; 278:29478–29486. [PubMed: 12746439]
4. Vassinova N, Kozyrev D. A method for direct cloning of Fur-regulated genes: identification of seven new Fur-regulated loci in *Escherichia coli*. Microbiology. 2000; 146:3171–3182. [PubMed: 11101675]
5. Monje-Casas F, Jurado J, Prieto-Alamo MJ, Holmgren A, Pueyo C. Expression analysis of the *nrdHIEF* operon from *Escherichia coli* Conditions that trigger the transcript level *in vivo* . J Biol Chem. 2001; 276:18031–18037. [PubMed: 11278973]
6. Gon S, Faulkner MJ, Beckwith J. *In vivo* requirement for glutaredoxins and thioredoxins in the reduction of the ribonucleotide reductases of *Escherichia coli*. Antioxid Redox Signal. 2006; 8:735–742. [PubMed: 16771665]
7. Lundin, D.; Torrents, E.; Furrer, E.; Larsson Birgander, P.; Sahlin, M.; Poole, AM.; Sjöberg, B-M. RNRdb: The ribonucleotide reductase database, Version 1.0. Dept. of Molecular Biology & Functional Genetics, Stockholm University; Stockholm, Sweden: 2005.
8. Schimpff-Weiland G, Follmann H, Auling G. A new manganese-activated ribonucleotide reductase found in gram-positive bacteria. Biochem Biophys Res Commun. 1981; 102:1276–1282. [PubMed: 7032519]
9. Auling G, Thaler M, Diekmann H. Parameters of unbalanced growth and reversible inhibition of deoxyribonucleic acid synthesis in *Brevibacterium ammoniagenes* ATCC 6872 induced by depletion of Mn^{2+} Inhibitor studies on the reversibility of deoxyribonucleic acid synthesis. Arch Microbiol. 1980; 127:105–114. [PubMed: 6158925]
10. Willing A, Follmann H, Auling G. Ribonucleotide reductase of *Brevibacterium ammoniagenes* is a manganese enzyme. Eur J Biochem. 1988; 170:603–611. [PubMed: 2828045]
11. Huque Y, Fieschi F, Torrents E, Gibert I, Eliasson R, Reichard P, Sahlin M, Sjöberg BM. The active form of the R2F protein of class Ib ribonucleotide reductase from *Corynebacterium ammoniagenes* is a diferric protein. J Biol Chem. 2000; 275:25365–25371. [PubMed: 10801858]
12. Jordan A, Pontis E, Atta M, Krook M, Gibert I, Barbe J, Reichard P. A second class I ribonucleotide reductase in *Enterobacteriaceae*: Characterization of the *Salmonella typhimurium* enzyme. Proc Natl Acad Sci USA. 1994; 91:12892–12896. [PubMed: 7809142]
13. Fieschi F, Torrents E, Toulokhonova L, Jordan A, Hellman U, Barbe J, Gibert I, Karlsson M, Sjöberg BM. The manganese-containing ribonucleotide reductase of *Corynebacterium ammoniagenes* is a class Ib enzyme. J Biol Chem. 1998; 273:4329–4337. [PubMed: 9468481]
14. Abbouni B, Oehlmann W, Stolle P, Pierik AJ, Auling G. Electron paramagnetic resonance (EPR) spectroscopy of the stable-free radical in the native metallo-cofactor of the manganese-ribonucleotide reductase (Mn-RNR) of *Corynebacterium glutamicum*. Free Radic Res. 2009; 43:943–950. [PubMed: 19707921]
15. Ogata H, Stolle P, Stehr M, Auling G, Lubitz W. Crystallization and preliminary x-ray analysis of the small subunit (R2F) of native ribonucleotide reductase from *Corynebacterium ammoniagenes*. Acta Cryst Section F. 2009; 65:878–880.
16. Griepenburg U, Blasczyk K, Kappl R, Hüttermann J, Auling G. A divalent metal site in the small subunit of the manganese-dependent ribonucleotide reductase of *Corynebacterium ammoniagenes*. Biochemistry. 1998; 37:7992–7996. [PubMed: 9609691]
17. Oka T, Udagawa K, Kinoshita S. Unbalanced growth death due to depletion of Mn^{2+} in *Brevibacterium ammoniagenes*. J Bacteriol. 1968; 96:1760–1767. [PubMed: 5726310]
18. Grass G, Franke S, Taudte N, Nies DH, Kucharski LM, Maguire ME, Rensing C. The metal permease ZupT from *Escherichia coli* is a transporter with a broad substrate spectrum. J Bacteriol. 2005; 187:1604–1611. [PubMed: 15716430]
19. Anjem A, Varghese S, Imlay JA. Manganese import is a key element of the OxyR response to hydrogen peroxide in *Escherichia coli*. Mol Microbiol. 2009; 72:844–858. [PubMed: 19400769]
20. Eriksson M, Jordan A, Eklund H. Structure of *Salmonella typhimurium* nrdF ribonucleotide reductase in its oxidized and reduced forms. Biochemistry. 1998; 37:13359–13369. [PubMed: 9748343]

21. Högbom M, Huque Y, Sjöberg BM, Nordlund P. Crystal structure of the di-iron/radical protein of ribonucleotide reductase from *Corynebacterium ammoniagenes*. Biochemistry. 2002; 41:1381–1389. [PubMed: 11802741]
22. Atkin CL, Thelander L, Reichard P, Lang G. Iron and free-radical in ribonucleotide reductase - exchange of iron and Mössbauer-spectroscopy of protein-B2 subunit of *Escherichia coli* enzyme. J Biol Chem. 1973; 248:7464–7472. [PubMed: 4355582]
23. Cotruvo JA Jr, Stubbe J. NrdI, a flavodoxin involved in maintenance of the diferric-tyrosyl radical cofactor in *Escherichia coli* class Ib ribonucleotide reductase. Proc Natl Acad Sci USA. 2008; 105:14383–14388. [PubMed: 18799738]
24. Wu CH, Jiang W, Krebs C, Stubbe J. YfaE, a ferredoxin involved in diferric-tyrosyl radical maintenance in *Escherichia coli* ribonucleotide reductase. Biochemistry. 2007; 46:11577–11588. [PubMed: 17880186]
25. Hristova D, Wu CH, Stubbe J. Importance of the maintenance pathway in the regulation of the activity of *Escherichia coli* ribonucleotide reductase. Biochemistry. 2008; 47:3989–3999. [PubMed: 18314964]
26. Roca I, Torrents E, Sahlin M, Gibert I, Sjöberg BM. NrdI essentiality for class Ib ribonucleotide reduction in *Streptococcus pyogenes*. J Bacteriol. 2008; 190:4849–4858. [PubMed: 18502861]
27. Massey V. Activation of molecular oxygen by flavins and flavoproteins. J Biol Chem. 1994; 269:22459–22462. [PubMed: 8077188]
28. McGee DPC, Vargeese C, Zhai Y, Kirschenheuter GP, Settle A, Sieden CR, Pieken WA. Efficient synthesis of 2′-amino-2′-deoxypyrimidine 5′-triphosphates. Nucleosides Nucleotides. 1995; 14:1329–1339.
29. Artin, EJ. PhD Thesis. Massachusetts Institute of Technology; Cambridge, MA: 2006. Mechanistic studies of the class I ribonucleotide reductase from *Escherichia coli*.
30. Fish WW. Rapid colorimetric micromethod for the quantitation of complexed iron in biological samples. Methods Enzymol. 1988; 158:357–364. [PubMed: 3374387]
31. Pierce BS, Hendrich MP. Local and global effects of metal binding within the small subunit of ribonucleotide reductase. J Am Chem Soc. 2005; 127:3613–3623. [PubMed: 15755183]
32. Parkin SE, Chen S, Ley BA, Mangravite L, Edmondson DE, Huynh BH, Bollinger JM Jr. Electron injection through a specific pathway determines the outcome of oxygen activation at the diiron cluster in the F208Y mutant of *Escherichia coli* ribonucleotide reductase protein R2. Biochemistry. 1998; 37:1124–1130. [PubMed: 9454605]
33. Steeper JR, Steuart CD. A rapid assay for CDP reductase activity in mammalian cell extracts. Anal Biochem. 1970; 34:123–130. [PubMed: 5440901]
34. Seyedsayamdost MR, Xie J, Chan CTY, Schultz PG, Stubbe J. Site-specific insertion of 3-aminotyrosine into the α2 subunit of *E. coli* ribonucleotide reductase: Direct evidence for involvement of Y730 and Y731 in radical propagation. J Am Chem Soc. 2007; 129:15060–15071. [PubMed: 17990884]
35. Bollinger JM Jr, Tong WH, Ravi N, Huynh BH, Edmondson DE, Stubbe J. Use of rapid kinetics methods to study the assembly of the diferric-tyrosyl radical cofactor of *Escherichia coli* ribonucleotide reductase. Methods Enzymol. 1995; 258:278–303. [PubMed: 8524156]
36. Malmström BG, Reinhammar B, Vanngard T. The state of copper in stellacyanin and laccase from the lacquer tree Rhus vernicifera. Biochim Biophys Acta. 1970; 205:48–57. [PubMed: 4314765]
37. Styring SA, Rutherford AW. The microwave power saturation of SII_{slow} varies with the redox state of the oxygen-evolving complex in photosystem II. Biochemistry. 1988; 27:4915–4923.
38. Khangulov SV, Barynin VV, Antonyuk-Barynina SV. Manganese-containing catalase from *Thermus thermophilus* peroxide-induced redox transformation of manganese ions in presence of specific inhibitors of catalase activity. Biochim Biophys Acta. 1990; 1020:25–33.
39. Meier AE, Whittaker MM, Whittaker JW. EPR polarization studies on Mn catalase from *Lactobacillus plantarum*. Biochemistry. 1996; 35:348–360. [PubMed: 8555195]
40. Khangulov SV, Barynin VV, Voevodskaya NV, Grebenko AI. ESR spectroscopy of the binuclear cluster of manganese ions in the active center of Mn-catalase from *Thermus thermophilus*. Biochem Biophys Res Commun. 1990; 1020:305–310.

41. Whittaker MM, Barynin VV, Antonyuk SV, Whittaker JW. The oxidized (3,3) state of manganese catalase. Comparison of enzymes from *Thermus thermophilus* and *Lactobacillus plantarum*. Biochemistry. 1999; 38:9126–9136. [PubMed: 10413487]
42. Ehrenberg A, Reichard P. Electron spin resonance of the iron-containing protein B2 from ribonucleotide reductase. J Biol Chem. 1972; 247:3485–3488. [PubMed: 4337857]
43. Torrents E, Sahlin M, Biglino D, Gräslund A, Sjöberg BM. Efficient growth inhibition of *Bacillus anthracis* by knocking out the ribonucleotide reductase tyrosyl radical. Proc Natl Acad Sci USA. 2005; 102:17946–17951. [PubMed: 16322104]
44. Nyholm S, Thelander L, Gräslund A. Reduction and loss of the iron center in the reaction of the small subunit of mouse ribonucleotide reductase with hydroxyurea. Biochemistry. 1993; 32:11569–11574. [PubMed: 8218224]
45. Gerez C, Fontecave M. Reduction of the small subunit of *Escherichia coli* ribonucleotide reductase by hydrazines and hydroxylamines. Biochemistry. 1992; 31:780–786. [PubMed: 1310046]
46. Waldo GS, Fronko RM, Penner-Hahn JE. Inactivation and reactivation of manganese catalase: oxidation-state assignments using x-ray absorption spectroscopy. Biochemistry. 1991; 30:10486–10490. [PubMed: 1657146]
47. Waldo GS, Penner-Hahn JE. Mechanism of manganese catalase peroxide disproportionation: determination of manganese oxidation states during turnover. Biochemistry. 1995; 34:1507–1512. [PubMed: 7849009]
48. Wu A, Penner-Hahn JE, Pecoraro VL. Structural, spectroscopic, and reactivity model for the manganese catalases. Chem Rev. 2004; 104:903–938. [PubMed: 14871145]
49. Fronko RM, Penner-Hahn JE, Bender CJ. EPR spectral evidence for a dinuclear active site in the *Lactobacillus plantarum* manganese catalase. J Am Chem Soc. 1988; 110:7554–7555.
50. Sjöberg BM, Gräslund A, Eckstein F. A substrate radical intermediate in the reaction between ribonucleotide reductase from Escherichia coli and 2′-azido-2′-deoxynucleoside diphosphates. J Biol Chem. 1983; 258:8060–8067. [PubMed: 6305969]
51. Fritscher J, Artin E, Wnuk S, Bar G, Robblee JH, Kacprzak S, Kaupp M, Griffin RG, Bennati M, Stubbe J. Structure of the nitrogen-centered radical formed during inactivation of E. coli ribonucleotide reductase by 2′-azido-2′-deoxyuridine-5′-diphosphate: trapping of the 3′-ketonucleotide. J Am Chem Soc. 2005; 127:7729–7738. [PubMed: 15913363]
52. Wieghardt K, Bossek U, Ventur D, Weiss J. Assembly and structural characterization of binuclear μ-oxo-di-μ-acetato bridged complexes of manganese(III) - Analogs of the di-iron(III) center in hemerythrin. J Chem Soc Chem Commun. 1985; 1985:347–349.
53. Sheats JE, Czernuszewicz RS, Dismukes GC, Rheingold AL, Petrouleas V, Stubbe J, Armstrong WH, Beer RH, Lippard SJ. Binuclear manganese(III) complexes of potential biological significance. J Am Chem Soc. 1987; 109:1435–1444.
54. Nordlund P, Sjöberg BM, Eklund H. Three-dimensional structure of the free radical protein of ribonucleotide reductase. Nature. 1990; 345:593–598. [PubMed: 2190093]
55. Kauppi B, Nielsen BB, Ramaswamy S, Larsen IK, Thelander M, Thelander L, Eklund H. The three-dimensional structure of mammalian ribonucleotide reductase protein R2 reveals a more-accessible iron-radical site than Escherichia coli R2. J Mol Biol. 1996; 262:706–720. [PubMed: 8876648]
56. Jiang W, Yun D, Saleh L, Barr EW, Xing G, Hoffart LM, Maslak MA, Krebs C, Bollinger JMJ. A manganese(IV)/iron(III) cofactor in *Chlamydia trachomatis* ribonucleotide reductase. Science. 2007; 316:1188–1191. [PubMed: 17525338]
57. Jiang W, Xie J, Nørgaard H, Bollinger JM Jr, Krebs C. Rapid and quantitative activation of *Chlamydia trachomatis* ribonucleotide reductase by hydrogen peroxide. Biochemistry. 2008; 47:4477–4483. [PubMed: 18358006]
58. Whittaker MM, Barynin VV, Igarashi T, Whittaker JW. Outer sphere mutagenesis of *Lactobacillus plantarum* manganese catalase disrupts the cluster core: Mechanistic implications. Eur J Biochem. 2003; 270:1102–1116. [PubMed: 12631270]
59. Dismukes GC. Manganese enzymes with dinuclear active sites. Chem Rev. 1996; 96:2909–2926. [PubMed: 11848845]

60. Antonyuk SV, Melik-Adamyan VR, Popov AN, Lamzin VS, Hempstead PD, Harrison PM, Artymyuk PJ, Barynin VV. Three-dimensional structure of the enzyme dimanganese catalase from *Thermus thermophilus* at 1 Å resolution. Cryst Rep. 2000; 45:105–116.
61. Barynin VV, Whittaker MM, Antonyuk SV, Lamzin VS, Harrison PM, Artymiuk PJ, Whittaker JW. Crystal structure of manganese catalase from *Lactobacillus plantarum*. Structure. 2001; 9:725–738. [PubMed: 11587647]
62. Andersson ME, Hogbom M, Rinaldo-Matthis A, Andersson KK, Sjöberg BM, Nordlund P. The crystal structure of an azide complex of the diferrous R2 subunit of ribonucleotide reductase displays a novel carboxylate shift with important mechanistic implications for diiron-catalyzed oxygen activation. J Am Chem Soc. 1999; 121:2346–2352.
63. Boelrijk AEM, Dismukes GC. Mechanism of hydrogen peroxide dismutation by a dimanganese catalase mimic: dominant role of an intramolecular base on substrate binding affinity and rate acceleration. Inorg Chem. 2000; 39:3020–3028. [PubMed: 11196896]
64. Gelasco A, Kirk ML, Kampf JW, Pecoraro VL. The $[Mn_2(2\text{-OHsalpn})_2]^{2-,-,0,+}$ system: Synthesis, structure, spectroscopy, and magnetism of the first structurally characterized dinuclear manganese series containing four distinct oxidation states. Inorg Chem. 1997; 36:1829–1837. [PubMed: 11669787]
65. Silva KE, Elgren TE, Que LJ, Stankovich MT. Electron transfer properties of the R2 protein of ribonucleotide reductase from *Escherichia coli*. Biochemistry. 1995; 34:14093–14103. [PubMed: 7578006]
66. Horner O, Anxolabéhère-Mallart E, Charlot MF, Tchertanov L, Guilhem J, Mattioli TA, Boussac A, Girerd JJ. A new manganese dinuclear complex with phenolate ligands and a single unsupported oxo bridge. Storage of two positive charges within less than 500 mV Relevance to photosynthesis. Inorg Chem. 1999; 38:1222–1232. [PubMed: 11670906]
67. Yun D, Garcia-Serres R, Chicalese BM, An YH, Huynh BH, Bollinger JM Jr. (μ-1,2-peroxo)diiron(III/III) complex as a precursor to the diiron(III/IV) intermediate X in the assembly of the iron-radical cofactor of ribonucleotide reductase from mouse. Biochemistry. 2007; 46:1925–1932. [PubMed: 17256972]
68. Bollinger JM Jr, Tong WH, Ravi N, Huynh BH, Edmondson DE, Stubbe J. Mechanism of assembly of the tyrosyl radical-diiron(III) cofactor of *Escherichia coli* ribonucleotide reductase. 2 Kinetics of the excess Fe^{2+} reaction by optical, EPR, and Mössbauer spectroscopies. J Am Chem Soc. 1994; 116:8015–8023.
69. Bollinger JM Jr, Tong WH, Ravi N, Huynh BH, Edmondson DE, Stubbe J. Mechanism of assembly of the tyrosyl radical-diiron(III) cofactor of *Escherichia coli* ribonucleotide reductase. 3 Kinetics of the limiting Fe^{2+} reaction by optical, EPR, and Mössbauer spectroscopies. J Am Chem Soc. 1994; 116:8024–8032.
70. Baldwin J, Krebs C, Ley BA, Edmondson DE, Huynh BH, Bollinger JM Jr. Mechanism of rapid electron transfer during oxygen activation in the R2 subunit of *Escherichia coli* ribonucleotide reductase. 1 Evidence for a transient tryptophan radical. J Am Chem Soc. 2000; 122:12195–12206.
71. Bollinger JM Jr, Edmondson DE, Huynh BH, Filley J, Norton JR, Stubbe J. Mechanism of assembly of the tyrosyl radical dinuclear iron cluster cofactor of ribonucleotide reductase. Science. 1991; 253:292–298. [PubMed: 1650033]
72. Fee JA. Regulation of *sod* genes in *Escherichia coli*: relevance to superoxide dismutase function. Mol Microbiol. 1991; 5:2599–2610. [PubMed: 1779751]
73. Meier B, Barra D, Bossa F, Calabrese L, Rotilio G. Synthesis of either Fe- or Mn-superoxide dismutase with an apparently identical protein moiety by an anaerobic bacterium dependent on the metal supplied. J Biol Chem. 1982; 257:13977–13980. [PubMed: 7142189]
74. Liu A, Pötsch S, Davydov A, Barra AL, Rubin H, Gräslund A. The tyrosyl free radical of recombinant ribonucleotide reductase from *Mycobacterium tuberculosis* is located in a rigid hydrophobic pocket. Biochemistry. 1998; 37:16369–16377. [PubMed: 9819229]

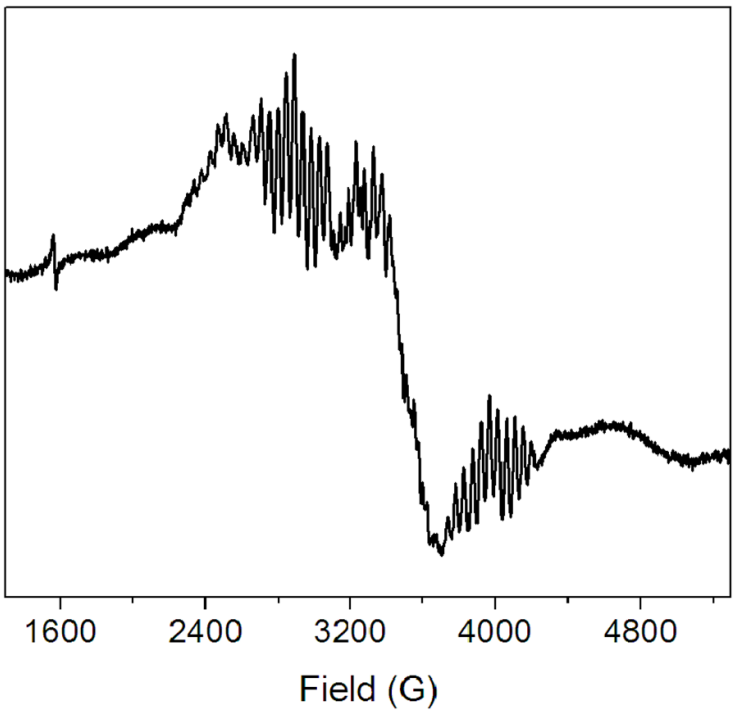

FIGURE 1.

EPR spectrum at 20 K of Mn^{II}_2-NrdF (40 μM). ApoNrdF was incubated with 4 Mn^{II}/β2 and mononuclear Mn^{II} was removed by Sephadex G25. The resulting protein contained 3.4 ± 0.2 Mn/β2 by atomic absorption spectroscopy.

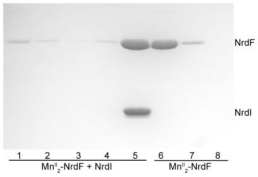

FIGURE 2.

Mn^{II}_2-NrdF interacts strongly with NrdI. Lanes 1–5: Mn^{II}_2-NrdF was incubated with 2 $NrdI_{ox}/\beta 2$ and loaded onto a Ni affinity column. Lane 1: flowthrough; lanes 2–5: washes with Buffer B containing 0, 10, 50, and 250 mM imidazole, respectively. Equal volumes of each sample were loaded onto the gel. Lanes 6–8: Mn^{II}_2-NrdF in the absence of NrdI does not bind to the Ni column. Flowthrough (lane 6), wash with Buffer B (lane 7), wash with Buffer B containing 10 mM imidazole (lane 8).

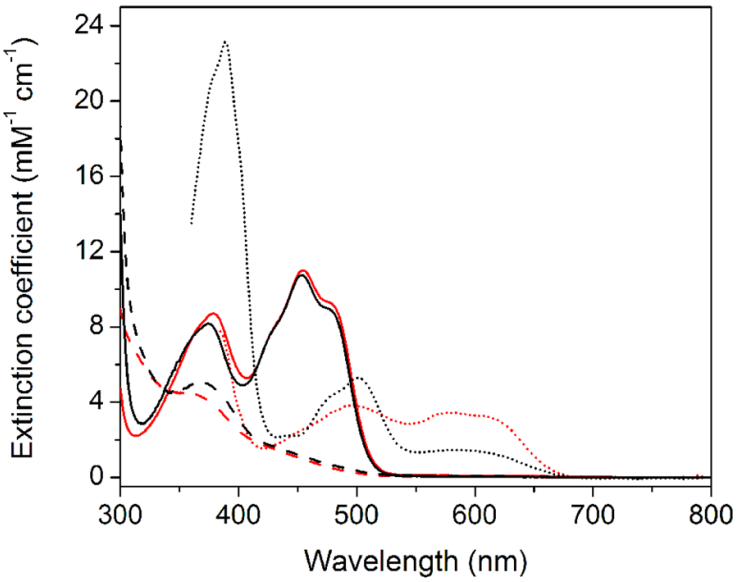

FIGURE 3.

Spectra of the ox (solid lines), sq (dotted lines), and hq (dashed lines) forms of NrdI in the presence (black) and absence (red) of apoNrdF, in Buffer C. The spectra of the neutral and anionic sq forms were estimated as described in Materials and Methods.

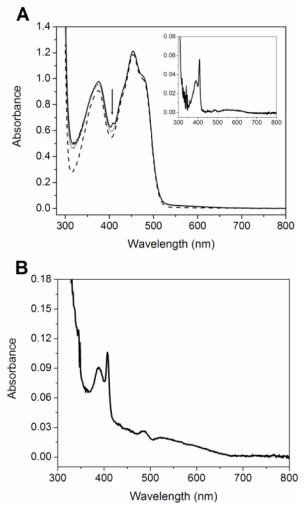

FIGURE 4.

Visible spectra of dimanganese-Y• NrdF. A) Visible spectra of 50 μM Mn^{II}_2-NrdF reconstituted with 100 μM $NrdI_{hq}$ and 1 mM O_2 in Buffer B (solid line); 50 μM Mn^{II}_2-NrdF with 100 μM $NrdI_{ox}$ (dashed line); and dimanganese-Y• NrdF after incubation with 50 mM HU for 8 min (dotted line). The arrow indicates the characteristic feature of Y• at 408 nm. Inset: Spectrum of Y•, obtained by subtraction of the spectrum of HU-treated NrdF from that of dimanganese-Y• NrdF. The presence of features at 500–700 nm in this difference spectrum suggests partial reduction of the Mn cluster by HU. B) Spectrum of the dimanganese-Y• cofactor, obtained by subtraction of the spectrum of Mn^{II}_2-NrdF in the presence of $NrdI_{ox}$ from that of dimanganese-Y• NrdF.

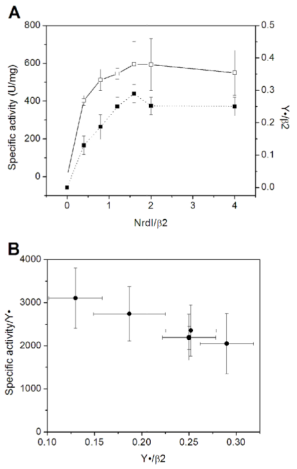

FIGURE 5.

Specific activity, Y•/β2, and specific activity/Y• of dimanganese-Y• NrdF assembled with increasing concentrations of $NrdI_{hq}$. A) SA (empty squares) and Y•/β2 (filled squares) are dependent on $NrdI_{hq}$ concentration in the assembly reaction. Mn^{II}_2-NrdF was preincubated with 0, 0.4, 0.8, 1.2, 1.6, 2, or 4 $NrdI_{hq}$/β2, in Buffer B and exposed to excess O_2. Y• was determined by EPR spin quantitation as described in Materials and Methods. Error bars indicate standard deviations of at least 2 independent experiments. B) SA/Y• plotted against Y•/β2 from data in Figure 5A.

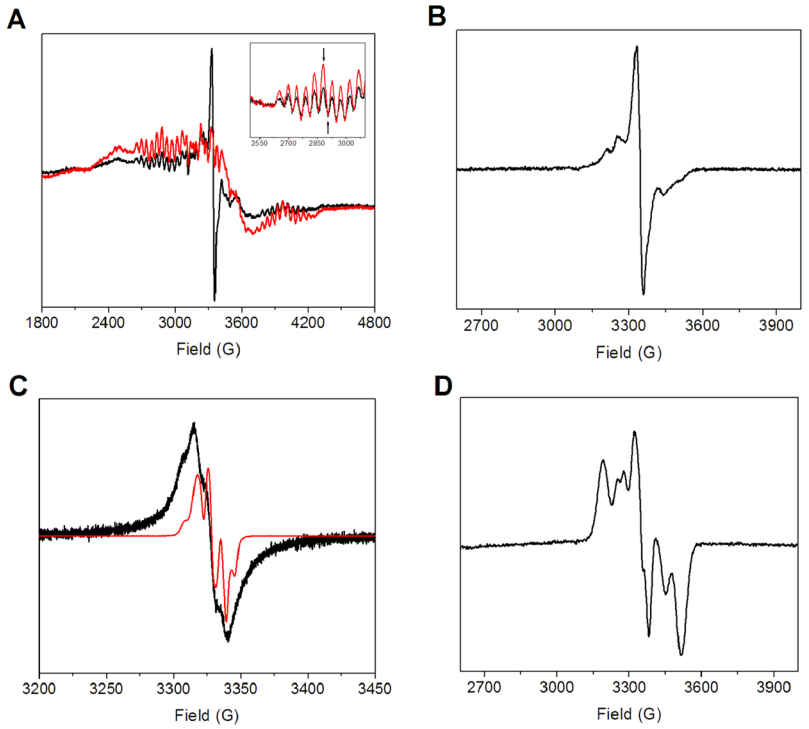

FIGURE 6.

EPR spectra of dimanganese-Y• NrdF. A) Comparison of the EPR spectra at 20 K of dimanganese-Y• NrdF and Mn^{II}_2-NrdF in the presence of $NrdI_{ox}$. In black, Mn^{II}_2-NrdF (50 μM) was reconstituted with 2 $NrdI_{hq}$/β2 (100 μM) and 1 mM O_2. In red, an identical sample, except $NrdI_{hq}$ was oxidized prior to addition of Mn^{II}_2-NrdF (control). A small amount of mononuclear Mn^{II} is visible at g = 2.0054 (3345 G). Inset: Expansion of the 2500–3100 G region to show the decrease in Mn^{II}_2 hyperfine intensity upon cofactor assembly. The arrows indicate the peak-to-trough intensity used to compare Mn^{II}_2 cluster concentrations. B) EPR spectrum at 20 K of dimanganese-Y• NrdF (50 μM) after EDTA and Sephadex G25 treatment, and after subtraction of a buffer sample. C) Comparison of the 77 K EPR spectra of EDTA-treated Mn^{III}_2-Y• NrdF (black, acquired at 1 mW power) and Fe^{III}_2-Y• NrdF (red, 50 μW power), with the vertical scales normalized for sample concentration and spectrometer settings except for power. D) EPR spectrum at 3.6 K of EDTA-treated Mn^{III}_2-NrdF, after subtraction of a buffer sample.

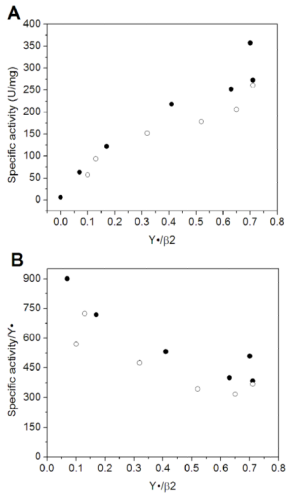

FIGURE 7.

Specific activity, Y•/β2, and SA/Y• for Fe^{III}_2-Y• NrdF. A) Correlation of specific activity and Y•/β2. ApoNrdF was preincubated anaerobically with 0, 0.6, 1, 2, 3, 4, or 5 Fe^{II}/β2 followed by addition of 3.5 O_2/β2. Data is shown for two sets of independent experiments (filled and open circles). SAs were determined using the radioactive assay. Y•/β2 was determined by EPR spin quantitation. Errors in the SA and Y• determinations are estimated at <10%. B) SA/Y• plotted against Y•/β2.

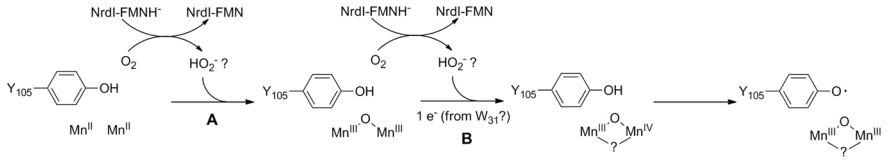

SCHEME 1.
Proposed mechanism for formation of Mn^{III}_2-Y• NrdF by $NrdI_{hq}$ and O_2.

TABLE 1

EPR relaxation properties of the Mn- and Fe-associated Y• in *E. coli* NrdF compared with those of Fe-associated Y•s of other NrdF proteins

	$P_{1/2}$ (mW)	b
Ec MnNrdF		
3.6 K	1.6 ± 0.2	0.91 ± 0.02
77 K	>100[a]	ND[b]
Ec FeNrdF		
3.6 K	0.03 ± 0.01	0.98 ± 0.03
77 K	0.47 ± 0.05	0.83 ± 0.01
Mt FeNrdF[c]		
5 K	0.01	0.78
77 K	0.72	1.25
St FeNrdF[d]		
95 K	3.7	1
Ca FeNrdF[d]		
95 K	1.3	1

[a] Signal only 10% saturated at 100 mW.

[b] ND – not determined.

[c] Ref. 74.

[d] Ref. 11.